analytical chemistry

pubs.acs.org/ac Article

Single-Atom Ruthenium Biomimetic Enzyme for Simultaneous Electrochemical Detection of Dopamine and Uric Acid

Xiaoli Xie, Dong Ping Wang, Chunxian Guo, Yuhang Liu, Qianghai Rao, Fangming Lou, Qiannan Li, Yongqiang Dong, Qunfang Li,* Hong Bin Yang,* and Fang Xin Hu*

Cite This: *Anal. Chem.* 2021, 93, 4916−4923 Read Online

ACCESS | Metrics & More | Article Recommendations | Supporting Information

ABSTRACT: Single-atom catalysts have attracted numerous attention due to the high utilization of metallic atoms, abundant active sites, and highly catalytic activities. Herein, a single-atom ruthenium biomimetic enzyme (Ru-Ala-C_3N_4) is prepared by dispersing Ru atoms on a carbon nitride support for the simultaneous electrochemical detection of dopamine (DA) and uric acid (UA), which are coexisting important biological molecules involving in many physiological and pathological aspects. The morphology and elemental states of the single-atom Ru catalyst are studied by transmission electron microscopy, energy dispersive X-ray elemental mapping, high-angle annular dark field−scanning transmission electron microscopy, and high-resolution X-ray photoelectron spectroscopy. Results show that Ru atoms atomically disperse throughout the C_3N_4 support by Ru−N chemical bonds. The electrochemical characterizations indicate that the Ru-Ala-C_3N_4 biosensor can simultaneously detect the oxidation of DA and UA with a separation of peak potential of 180 mV with high sensitivity and excellent selectivity. The calibration curves for DA and UA range from 0.06 to 490 and 0.5 to 2135 μM with detection limits of 20 and 170 nM, respectively. Moreover, the biosensor was applied to detect DA and UA in real biological serum samples using the standard addition method with satisfactory results.

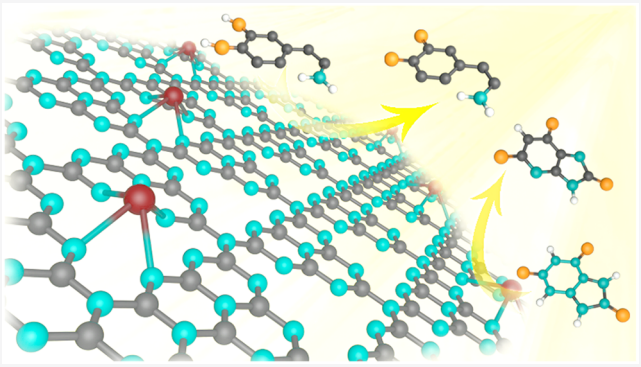

INTRODUCTION

Dopamine (DA) and uric acid (UA) are important electrochemically active molecules commonly coexisting in the human body. Dopamine (DA) is a primary catecholamine neurotransmitter molecule with a basal concentration of about 0.01−1 μM, transferring the message of excitement and happiness in the renal, cardiovascular, and central nervous systems, and plays a vital role in many physiological and pathological aspects.[1] However, abnormalities of DA levels may lead to tardive dyskinesia and neuroendocrine disorders, such as Parkinson's disease and schizophrenia.[2] Uric acid (UA) is the final product of purine metabolism that is present in human serum and urine with a concentration of 0.2−0.5 mM.[3,4] The excessive accumulation of UA may not only result in gout and hyperuricemia but also inhibit insulin signaling and therefore induce insulin resistance.[5] As is known to all, DA and UA commonly coexist in the human body. Therefore, the simultaneous detection of DA and UA is of great importance for analytical application and diagnostic research. However, it is still a great challenge to simultaneously monitor DA and UA due to their similar structures, and their redox potentials are too close to each other and largely overlap in many cases.

Many approaches have been developed for determination of DA and UA in the past decades, including high performance liquid chromatography−mass spectrometry,[6,7] fluorescence,[8,9] spectrophotometry,[10] and so on. However, these methods suffer from complicated, expensive, and time-consuming processes and also require specialized instrumentation. Comparing with these methods mentioned above, electrochemical techniques possess the features of simple operation, quick response, low cost, and good selectivity,[11−14] which are expected to reach the simultaneous detection of DA and UA. Several nanomaterials have been reported to monitor DA and UA, such as carbon nanomaterials,[15−18] metal nanomaterials,[19−21] polymer nanomaterials,[22−24] self-assembled monolayers,[25] and ionic liquids.[26] Although electrochemical sensors based on these materials have been successfully used for the oxidation potential separation of DA and UA, they still suffer from narrow detection ranges and low sensitivities.

Recently, single-atom catalysts (SACs), exhibiting full atom utilization have demonstrated promising applications in

Received: December 11, 2020
Accepted: March 1, 2021
Published: March 10, 2021

electrocatalysis due to their advantages of abundant active sites and unique catalytic functions.[27] Among the noble metals, Ruthenium (Ru)-based single-atom catalysts are applied in ammonia synthesis,[28] oxidative cyanation,[29] CO_2 hydrogenation systems,[30] and oxygen[31−33] and hydrogen evolution reactions.[34] However, preparing catalysts to the single-atom level is difficult because they are thermodynamically unstable and tend to aggregate into clusters or nanoparticles during the preparation process.[31] Monolayer graphitic carbon nitride (C_3N_4) is a typical two-dimensional nanomaterial with good biocompatibility, outstanding stability, and suitable energy band structure for electrochemical transformations, which provide an ideal matrix for immobilization of the metal atoms and fabrication of single atom catalysts.[35] Besides, nitrogen−carbon supported SACs such as metal−nitrogen−carbon (M−N−C) possess enzyme-like activity with high active site density and excellent electrical conductivity.[36] In our previous work, it is demonstrated that a nitrogen−carbon supported single-atom Co catalyst acts as biomimetic enzyme for UA molecule detection with a wide linear range and ultralow detection limit, which showed commendable activity.[13] Nevertheless, a single-atom catalyst for simultaneous electrochemical biomolecule detection has not been explored yet. It is expected that a single-atom Ru catalyst could be used as a functional material for the simultaneous electrochemical detection of DA and UA.

In this work, we design and fabricate a single-atom biomimetic enzyme comprising high-density Ru atoms dispersed on a C_3N_4 matrix (Ru-Ala-C_3N_4) for the simultaneous electrochemical detection of DA and UA. The material characterization and experiment are carried out to expound the structure, properties, and enzyme-like electrochemical activity of Ru-Ala-C_3N_4. Results show that the fabricated Ru-Ala-C_3N_4 biosensor achieves the simultaneous electrochemical detection of DA and UA with an extremely low detection limit of 20 and 170 nM, respectively, due to its abundant and efficient active sites. Besides, the biosensor modified with Ru-Ala-C_3N_4 biomimetic enzyme exhibited good reproducibility and stability, as well as great selectivity, and was successfully applied for detection of DA and UA in real biological serum samples.

EXPERIMENTAL SECTION

Chemicals. Melamine ($C_3H_6N_6$), L-alanine (L-Ala), ruthenium(III) chloride ($RuCl_3$), uric acid (UA), dopamine (DA), ascorbic acid (AA), potassium chloride (KCl), calcium chloride ($CaCl_2$), glucose (Glu), cysteine (Cys), glutathione (GSH), sodium carbonate (Na_2CO_3), sodium nitrite ($NaNO_2$), and Nafion were purchased from Sigma-Aldrich. Sodium sulfate (Na_2SO_4) was purchased from Aladdin. All of the other chemical reagents were purchased from Sigma-Aldrich and used directly without further purification. Buffer solutions with different pH values were prepared with 0.1 M NaH_2PO_4 and 0.1 M Na_2HPO_4 using a Mettler-Toledo pH meter. Deionized water (resistivity over 18 MΩ cm) from a Millipore Q water purification system was used in all experiments.

Apparatus. The electrochemical measurements are performed on a CHI 660e electrochemical workstation (CH Instruments, Chenhua Corp., China). A three-electrode system was applied including a working electrode modified by different materials, and a saturated calomel electrode (SCE) and platinum wire as the reference and counter electrodes, respectively. The crystal structure and morphology of the catalysts were examined by X-ray diffraction (XRD, Bruker AXS D8 Advance) with Cu Kα, radiation (λ = 1.5406 Å), transmission electron microscopy (TEM, JEOL JEM-2100F), scanning electron microscopy (SEM, Zeiss Merlin), energy dispersive X-ray (EDX, JEOL JED-2300 Analysis Station) elemental mapping, and atomic force microscopy (AFM, Bruker Dimension ICON). The chemical compositions and elemental states were carried out by high-resolution X-ray photoelectron spectroscopy (XPS) on an ESCALAB 250 photoelectron spectrometer (Thermo Fisher Scientific) using a monochromatic Al Kα X-ray beam (1486.6 eV). All binding energies were referenced to the C 1s peak (284.6 eV). The specific surface area was investigated based on a Brunauer−Emmett−Teller (BET) method using Autosorb 6B at liquid-nitrogen temperature.

Synthesis of Single Atom Ru-Ala-C_3N_4 Catalyst and Control Materials. In a typical synthesis of Ru-Ala-C_3N_4 catalyst,[37] $C_3H_6N_6$ (9 g), L-Ala (0.5 g), and $RuCl_3$ (0.05 g) were mixed homogeneously through ball milling. Then, the fine powder mixture underwent a pyrolysis process at 500 °C with a ramping rate of 2 °C min^{-1}, maintained at 500 °C for 2 h in a tubular furnace in a nitrogen atmosphere. Then, the Ru-Ala-C_3N_4 was obtained by cooling the furnace to room temperature under nitrogen protection.

As control materials, the C_3N_4 catalyst was obtained by pyrolyzing the fine powder of $C_3H_6N_6$ (9 g) following the above procedure. The Ala-C_3N_4 catalyst and Ru-C_3N_4 catalyst were prepared by pyrolyzing the mixture of $C_3H_6N_6$ (9 g) and Ala (0.5 g), and the mixture of $C_3H_6N_6$ (9 g) and $RuCl_3$ (0.05 g), respectively, according to similar procedures.

Preparation of the Electrode Modified with Ru-Ala-C_3N_4. To prepare the Ru-Ala-C_3N_4 biosensor, the glass carbon electrode (GCE, Ø = 3 mm) was sequentially polished by 0.3 and 0.05 μm alumina, followed by ultrasonic washing with ethanol and deionized water for 2 min to obtain a mirror like surface. Then 10 mg mL^{-1} Ru-Ala-C_3N_4 suspension was prepared using ethanol and deionized water mixture (1:4) as a dispersing agent by ultrasonic treatment for 30 min. The obtained Ru-Ala-C_3N_4 suspension (5 μL) was dropped on the clean GCE surface and dried at room temperature to prepare Ru-Ala-C_3N_4/GCE. The working electrode modified with Ru-Ala-C_3N_4 was applied to detect DA and UA simultaneously by cyclic voltammetry (CV) and differential pulse voltammetry (DPV) measurements. For comparison, C_3N_4/GCE, Ala-C_3N_4/GCE, and Ru-C_3N_4/GCE were also prepared with the same procedure.

RESULTS AND DISCUSSION

Characterization of the Ru-Ala-C_3N_4Catalyst. The single-atom Ru catalyst is prepared by pyrolyzing a mixture of melamine, L-Ala, and $RuCl_3$ under nitrogen protection (Figure 1a). The morphology and structure of the single-atom Ru catalyst are first characterized by TEM and SEM. Figure 1b, c shows a two-dimensional (2D) sheetlike structure with a smooth surface for Ru-Ala-C_3N_4, which exhibits a similar morphology feature to graphene. AFM measurement confirms the sheet morphology of Ru-Ala-C_3N_4 with a thickness of ∼1.2 nm (Figure 1d). The elemental mapping measurement indicates that the elements of C, N, and Ru are uniformly distributed in sample, and no local aggregation of Ru can be observed (Figure 1e). The high-angle annular dark field−scanning transmission electron microscopy (HAADF-STEM) image highlights isolated high-density bright spots disperse

https://dx.doi.org/10.1021/acs.analchem.0c05191
Anal. Chem. 2021, 93, 4916−4923

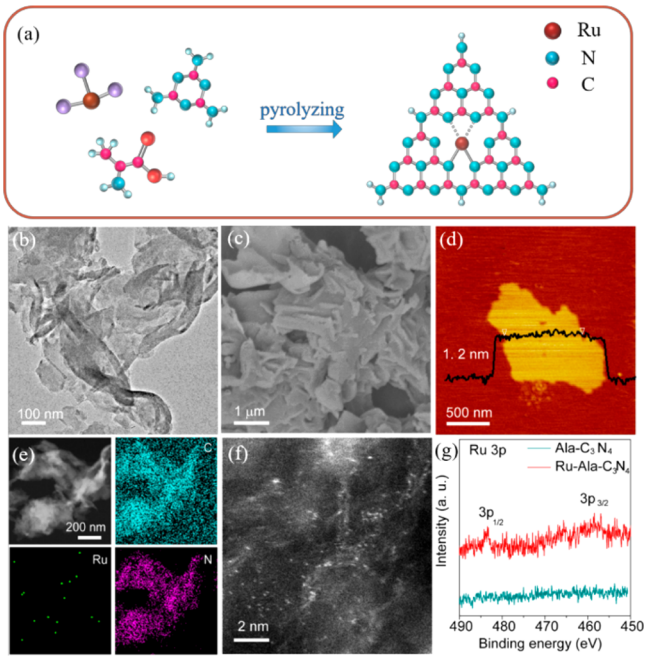

Figure 1. (a) Schematic illustration of single-atom Ru catalyst preparation. (b) TEM and (c) SEM images of Ru-Ala-C_3N_4. (d) AFM image and the corresponding cross-sectional profile of Ru-Ala-C_3N_4. (e) EDX elemental mapping and (f) HAADF-STEM image of Ru-Ala-C_3N_4. (g) High-resolution XPS image of Ru in the Ru-C_3N_4 and Ru-Ala-C_3N_4 catalyst.

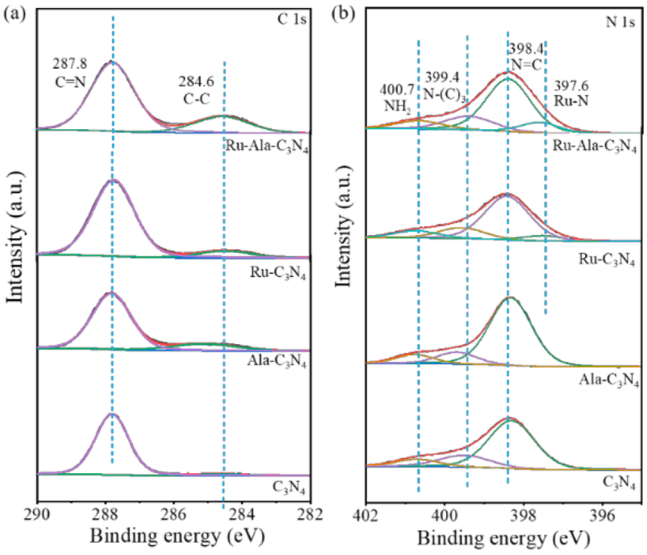

Figure 2. High-resolution XPS of (a) C 1s and (b) N 1s spectra of samples.

across the entire C_3N_4 support in Ru-Ala-C_3N_4, due to the single Ru atom having a larger atomic mass than C and N (Figure 1f).

XPS is performed to measure the compositions and chemical states of the electrocatalysts. Figure S1 shows the XPS survey spectrum of samples. The high-resolution of Ru 3p XPS spectrum of Ru-Ala-C_3N_4 displays two peaks centered at 465.1 and 483.5 eV, corresponding to the binding energy of Ru $3p_{3/2}$ and Ru $3p_{1/2}$, respectively. As displayed by the high-resolution C 1s spectra of Ru-Ala-C_3N_4, Ru-C_3N_4, Ala-C_3N_4, and C_3N_4 (Figure 2a), the incorporation of amino acid (L-Ala) and Ru atom leads to increase the content of sp^2 carbon (284.6 eV), which could facilitate the electron transfer of the sample in the chemical reaction. Figure 2b shows the N 1s of samples: all the samples bear the similar typical nitrogen species for carbon nitride (NH_2, N—$(C)_3$, N=C), whereas it is important to note that a new nitrogen peak (N 1s) emerges at 397.6 eV in the spectrum of Ru-Ala-C_3N_4 and Ru-C_3N_4 (Figure 2b), which can be assigned to the chemical bond of Ru−N, confirming the immobilization of the single atomically dispersed Ru atoms on the C_3N_4 matrix by Ru−N chemical bonds. XRD is employed to study the crystal structure of Ru-Ala-C_3N_4, Ru-C_3N_4, Ala-C_3N_4, and C_3N_4. As shown in Figure S2a, the metallic Ru diffraction peak is absent in XRD patterns of Ru-Ala-C_3N_4 and Ru-C_3N_4, and only (210) periodic arrangement in plane of C_3N_4 at 13.1° as well as (200) and (100) carbon diffraction peaks at 26.2° and 44.0° are observed, indicating that Ru is atomically dispersed in the C_3N_4 support.

Electrochemical Behaviors of DA and UA on the Modified Biosensor. First, we compare the CV and DPV responses of a series of control materials in 0.1 M PBS (pH 7.4) containing mixtures of 100 μM DA and 200 μM UA. CV results are shown in Figure S3, which reveals a broad and weak anodic peak toward the oxidation of DA and UA at Ala-C_3N_4/GCE and C_3N_4/GCE. The response of Ru-C_3N_4/GCE toward DA and UA is better than those of Ala-C_3N_4/GCE and C_3N_4/GCE, due to the enhanced catalytic activity of the Ru atom. Compared with the mentioned materials, Ru-Ala-C_3N_4/GCE exhibits two well-defined voltammetric peaks at potentials of approximately 170 and 350 mV with a remarkable increase in peak current for DA and UA, which can be assigned to the faster charge transfer rate of the Ru-Ala-C_3N_4 material, revealed by XPS measurement (Figure 2a). Besides, from the DPV response (Figure 3a, b), it can be concluded Ru-Ala-C_3N_4/GCE achieves the best performance for simultaneous detection of 100 μM DA and 200 μM UA, indicating the intrinsic superiority of the single-atom Ru biomimetic enzyme.

The electrochemical responses of Ru-Ala-C_3N_4/GCE toward DA and UA were further investigated (Figure 3c). After addition of 100 μM DA into PBS, a well-defined pair of redox peaks emerged at 170 and 120 mV (black curve of Figure 3c), respectively, which can be assigned to the oxidation of DA to dopamine quinone and the subsequent reduction of dopamine quinone to DA (lower inset of Figure 3d).[38] The tiny difference between oxidation and reduction potential demonstrates the excellent reversibility of DA on the Ru-Ala-C_3N_4 biomimetic enzyme. In the case of 200 μM UA (blue curve of Figure 3c), there appears a remarkable oxidation peak at 320 mV and a reduction peak at 250 mV due to the redox reaction between UA and urate on the Ru-Ala-C_3N_4 (upper inset of Figure 3d).[18]

Besides, the CV curve of the mixture of 100 μM DA and 200 μM UA records two well-defined voltammetric peaks at potentials of approximately 170 and 350 mV for DA and UA, respectively, with remarkable peak currents of 0.9 and 1.3 μA. A large separation of peak potentials (ΔE) of 180 mV (red line of Figure 3c) can be calculated for the electro-oxidation of DA and UA, ensuring the simultaneous detection of them. Besides, the existence of DA further enhances the response of UA as can be observed in Figure 3c, red curve. This may be ascribed to the fact that DA is an alkaline molecule, which can change the pH environment of the solution and increase the solubility of UA, and thus increase the response of UA. The electrocatalytic performance of Ru-Ala-C_3N_4/GCE is further

https://dx.doi.org/10.1021/acs.analchem.0c05191
Anal. Chem. 2021, 93, 4916−4923

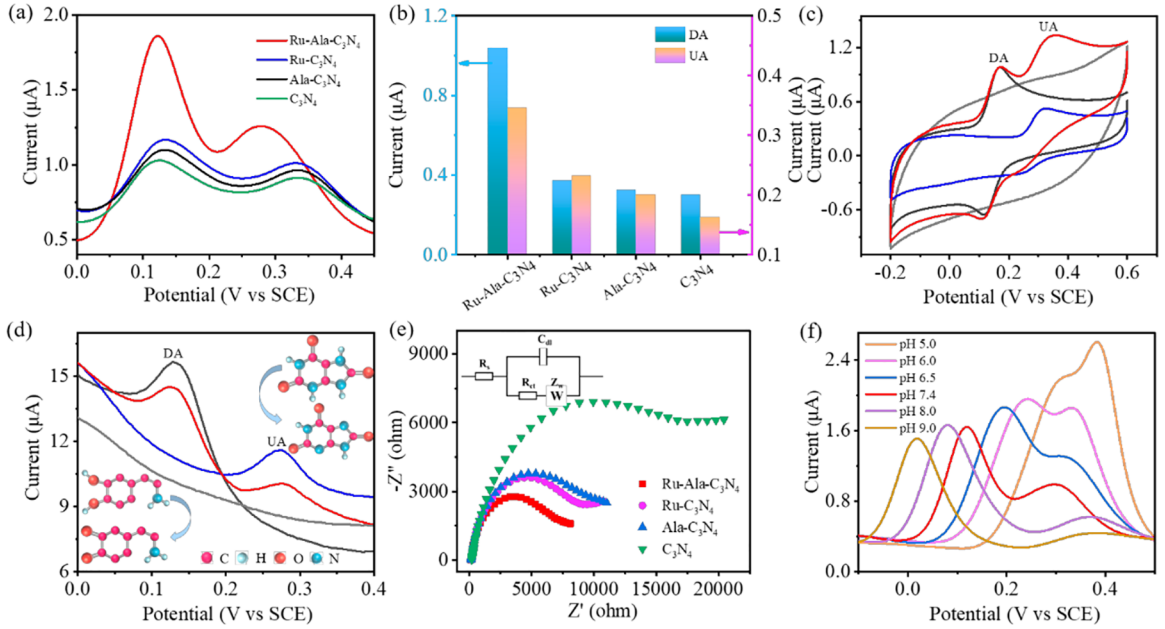

Figure 3. (a) DPVs of electrodes modified with different materials. (b) Current response of different materials for simultaneous detection of 100 μM DA and 200 μM UA. (c) CVs and (d) DPVs of the Ru-Ala-C_3N_4/GCE by adding 100 μM DA (black curve) and 200 μM UA (blue curve), with (red curve) and without (gray curve) a mixture of 100 μM DA and 200 μM UA in 0.1 M PBS (pH 7.4). (e) EIS of samples. (f) Influence of pH of test solution on the electrochemical response of the Ru-Ala-C_3N_4/GCE toward mixture of 100 μM DA and 200 μM UA.

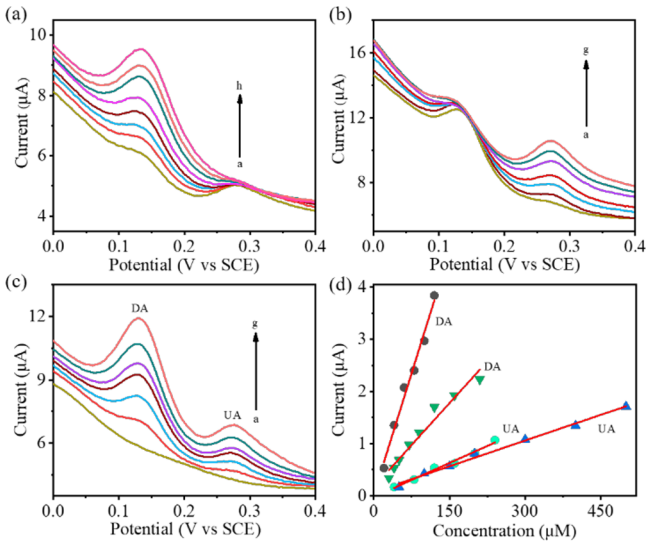

Figure 4. DPVs of the Ru-Ala-C_3N_4/GCE in 0.1 M PBS (pH 7.4) (a) containing 200 μM UA and individual concentrations of the DA (a–h) 30, 40, 50, 70, 90, 120, 160, and 210 μM, (b) containing 50 μM DA and individual concentrations of the UA (a–g) 50, 100, 150, 200, 300, 400, and 500 μM. (c) DPVs of the Ru-Ala-C_3N_4/GCE in 0.1 M PBS (pH 7.4) containing individual concentrations of the DA and UA mixture (DA 0, 20, 40, 60, 80, 100, and 120 μM; UA 0, 40, 80, 120, 160, 200, and 240 μM). (d) Plots of Ip vs concentration for individual (triangle) and simultaneous (dot) detection of DA and UA, respectively.

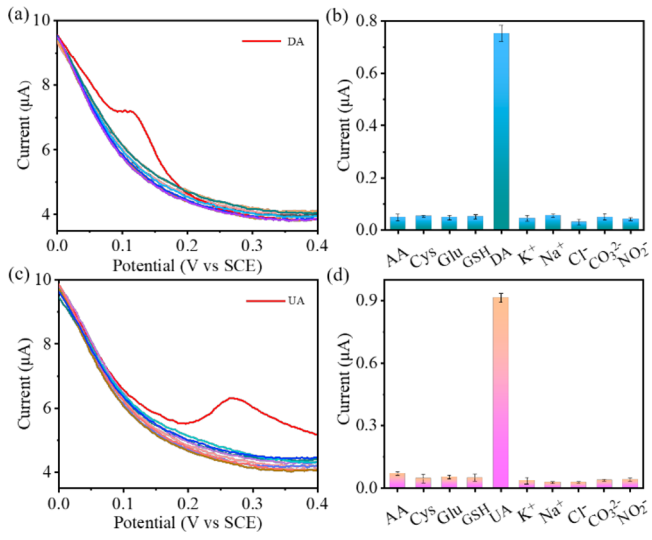

Figure 5. Selectivity of Ru-Ala-C_3N_4/GCE toward (a, b) DA and (c, d) UA.

verified by DPV measurement, Figure 3d clearly shows the oxidation peaks of DA and UA. These results indicate that the discrimination of DA and UA is feasible and Ru-Ala-C_3N_4/GCE can determine the two substances simultaneously.

The charge transport characteristics of C_3N_4, Ala-C_3N_4, Ru-C_3N_4, and Ru-Ala-C_3N_4 were investigated by electrochemical impedance spectroscopy (EIS) over a frequency range from 100 000 to 1 Hz at open circuit voltage with 5 mV amplitude voltage, using 5 mM $[Fe(CN)_6]^{3-/4-}$ in 0.1 M KCl solution as a redox probe. The interface charger transfer resistance (R_{ct}) values of C_3N_4/GCE, Ala-C_3N_4/GCE, Ru-C_3N_4/GCE, and Ru-Ala-C_3N_4/GCE were obtained as 14 281, 7328, 8190, and 5029 Ω, respectively, through fitting EIS spectra using the equivalent circuit (inset of Figure 3e). The dramatic reduction of R_{ct} indicates that the Ru-Ala-C_3N_4/GCE has a better electron transfer rate and electrocatalytic activity compared with C_3N_4/GCE, Ala-C_3N_4/GCE, and Ru-C_3N_4/GCE. The enhancement of electrochemical redox of DA and UA on Ru-Ala-C_3N_4/GCE might be ascribed as follows: on one hand, Ru-Ala-C_3N_4 could provide abundant active sites which are more favorable for the adsorption of small molecules like DA and

https://dx.doi.org/10.1021/acs.analchem.0c05191
Anal. Chem. 2021, 93, 4916–4923

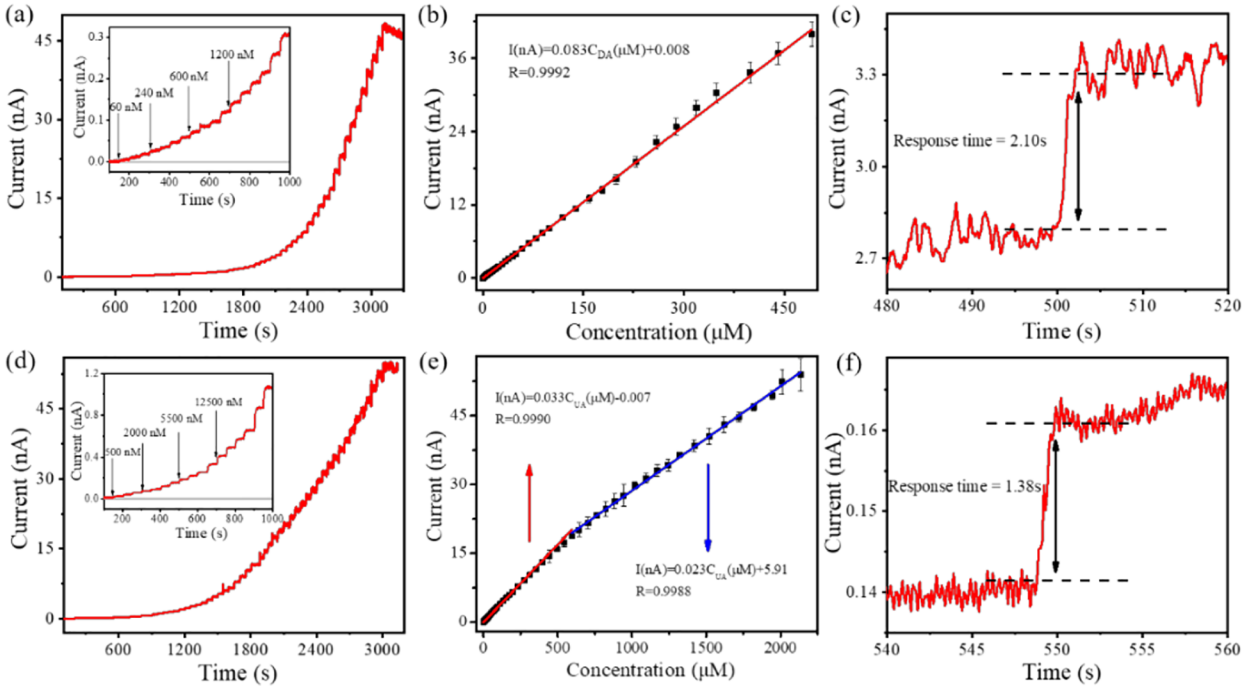

Figure 6. (a) Typical amperometric response ($I-t$) of Ru-Ala-C_3N_4/GCE to successive addition of DA at applied potentials of 0.2 V versus SCE in 0.1 M PBS (pH 7.4). (inset) $I-t$ with low concentrations of DA. (b) Calibration plot of steady-state current and (c) response time of Ru-Ala-C_3N_4/GCE to DA. (d) Typical amperometric responses of Ru-Ala-C_3N_4/GCE toward successive addition of UA at applied potentials of 0.32 V versus SCE in 0.1 M PBS (pH 7.4). (inset) Amperometric responses with low concentrations of UA. (e) Calibration plot of steady-state current and (f) response time of Ru-Ala-C_3N_4/GCE to UA.

Table 1. Comparison of the Sensing Performance of the Ru-Ala-C_3N_4 with That of Recently Reported Materials Towards the Simultaneous Detection of DA and UA[a]

	linear range (μM)		LOD (μM)		
materials	DA	UA	DA	UA	ref
nano-Au/P-TA	0.6−340	1.6−110	0.05	0.08	40
RGO-ZnO	1−70	3−330	0.33	1.08	41
Pt-CO@RGO	35−1500	5−800	0.051	0.172	42
Fe(III)P/MWCNTs	0.7−3600	5.8−1300	0.09	0.3	2
RGO/Pd@PPy	38−1647	1.4−219	0.056	0.047	43
PtNi@MoS_2	0.5−150	0.5−600	0.1	0.1	44
TiN-RGO	5−175	30−215	0.159	0.350	5
RGO-Ag/PANI	5−200	20−350	0.2	0.2	45
PPy hydrogel	0.08−250	0.25−400	0.044	0.046	46
Yb_2O_3-RGO	0.3−800	0.2−210	0.02	0.01	47
HNP-PtTi alloy	4−500	100−1000	3.2	5.3	48
Au/RGO	6.8−410	8.8−530	1.4	1.8	49
Ru-Ala-C_3N_4	0.06−490	0.5−2100	0.02	0.17	this work

[a]P-TA: poly(3-amino-5-mercapto-1,2,4-triazole). PANI: polyaniline. PPy: polypyrrole. Fe(III)P: iron(III)-porphyrin. HNP: hierarchical nanoporous. RGO: reduced graphene oxide.

UA due to Ru being atomically dispersed in the C_3N_4 support[13] and leading to the effective catalytic redox reaction of DA and UA. On the other hand, electron transfer between Ru-Ala-C_3N_4 and the electrode surface was significantly facilitated due to the excellent conductivity of the Ru atom and the increase of sp^2 carbons by doping with L-Ala.[39]

Table 2. Results for the Detection of DA and UA in Real Samples

sample	species	detected (μM)	added (μM)	found (μM)	recovery (%)
serum 1	UA	6.64	4	11.48	107.9
	DA		3	3.15	105.0
serum 2	UA	5.75	4	8.78	90.1
	DA		3	2.9	96.7
serum 3	UA	8.01	6.5	13.54	93.31
	DA		3	2.7	90.0

The effect of pH on the performance of the Ru-Ala-C_3N_4/GCE biosensor toward the simultaneous detection of DA and UA is investigated (Figure 3f). The separation of peak potentials of Ru-Ala-C_3N_4/GCE for DA and UA increases with pH changes from 5.0 to 7.4. When the pH value increases from 7.4 to 9.0, the response of DA and UA becomes harder and harder to separate. To achieve the best detection of both DA and UA, pH 7.4 is selected as the optimal value of the PBS for further experiments. In addition, pH 7.4 is closer to the pH of the bioenvironment, which is more suitable for DA and UA monitoring in biological systems.

Simultaneous Determination of DA and UA. The simultaneous detection of DA and UA on Ru-Ala-C_3N_4/GCE was carried out by DPV in 0.1 M PBS (pH 7.4). In the mixture solution, the concentration of one species varies while the concentration of another remains constant. Figure 4a depicts the DPV curves of the different DA concentrations containing 200 μM UA. As the concentration of DA increases from 30 to 210 μM, the oxidation peak shows an increase in current response at the potential of approximately 0.13 V. Similarly, Figure 4b reveals the peak current response increase with the concentration of UA changing from 50 to 500 μM while the

https://dx.doi.org/10.1021/acs.analchem.0c05191
Anal. Chem. 2021, 93, 4916−4923

solution contains 50 μM DA. For the simultaneous detection of DA and UA, Figure 4c displays the electrocatalytic oxidations of DA and UA mixtures at Ru-Ala-C_3N_4/GCE by increasing their concentrations. It can be observed two well-defined voltammetric peaks corresponding to the oxidation of DA and UA, respectively, appear at Ru-Ala-C_3N_4, and the peak currents increased in proportion to the concentrations of DA and UA. The calibration curves for the individual and simultaneous detection of DA and UA are shown in Figure 4d. Results indicate that the biosensor modified with Ru-Ala-C_3N_4 can realize simultaneous monitoring of DA and UA.

Interferences, Reproducibility, and Stability. The selectivity and anti-interference ability of the Ru-Ala-C_3N_4/GCE biosensor is carried out by testing 0.9 mM K^+, Na^+, Cl^-, CO_3^{2-}, NO_2^-, 500 μM AA, Cys, Glu, and GSH, which might coexist with DA and UA in biological systems. Result shows these species do not cause any noticeable interference to the response of 100 μM DA and 200 μM UA, as displayed in Figure 5, demonstrating an excellent selectivity and anti-interference ability of the Ru-Ala-C_3N_4/GCE biosensor toward the oxidation of DA and UA.

The reproducibility of Ru-Ala-C_3N_4/GCE is also investigated by DPV. For six independent electrodes, the RSD of the current response to 100 μM DA and 200 μM UA are 0.97% and 0.70%, respectively, indicating a good reproducibility of the Ru-Ala-C_3N_4/GCE biosensor. The repeatability of the Ru-Ala-C_3N_4/GCE biosensor is examined though nine successive measurements by one electrode, the RSD of the current response to 100 μM DA and 200 μM UA are 0.37% and 0.32%, respectively, indicating an excellent repeatability. Furthermore, the Ru-Ala-C_3N_4 biomimetic enzyme exhibits good stability toward DA and UA by retaining above 90.2% and 92.0% activity after storage for 30 days, respectively.

Amperometric Determination of DA and UA. The $I-t$ responses of the Ru-Ala-C_3N_4/GCE biosensor toward DA and UA are recorded in Figure 6. The response current is measured under the optimized conditions at successive addition of DA or UA into a stirred solution of 0.1 M PBS (pH 7.4). Figure 6a shows the $I-t$ of DA containing 100 μM UA. The current responses of DA increases linearly with increasing DA concentrations in the range of 0.06−490 μM, with a linear regression equation of I (nA) = 0.083C_{DA} (μM) + 0.008 (R = 0.9992) and a detection limit of 20 nM (Figure 6b). Figure 6d illustrates the $I-t$ of UA containing 50 μM DA. Two linear ranges of 0.5−595 and 595− 2135 μM are obtained for the UA detection, with the linear equations of I (nA) = 0.033C_{UA} (μM) − 0.007 (R = 0.9990) and I (nA) = 0.023C_{UA} (μM) + 5.91 (R = 0.9988), respectively. And the detection limit for UA is 170 nM calculated at a signal-to noise ratio of 3 (Figure 6e). Furthermore, the response time of DA and UA are recorded in Figure 6c and f, respectively. The modified electrode achieves 95% of the steady-current within 2.1 and 1.38 s for DA and UA. The prepared Ru-Ala-C_3N_4/GCE demonstrates a wider linear range and relatively low detection limit which are comparable with those previously reported in the literature (Table 1).

Real Sample Analysis. Serum examination is a convenient method to detect some disease indexes, which can quickly get the detection results. Herein, several serum samples are detected using standard addition method, and the potential application of a Ru-Ala-C_3N_4 biomimetic enzyme sensor for DA and UA detection is investigated. Results are shown in Table 2 and Figure S5. The recovery of UA and DA ranged from 90.1−107.9% and 90.0−105.0%, respectively, indicating that the proposed method could be effectively used for the detection of DA and UA in real biological samples. In addition, the results for real biological serum samples determined by the prepared Ru-Ala-C_3N_4 biosensor are compared with the standard assay for UA carried out by a fully automatic biochemical analyzer (HITACHI LABOSPECT 008). The calculated accuracy of the prepared sensor is 94.3% (RSD = 4.9%).

CONCLUSIONS

In summary, we present a single-atom Ru catalyst as a biomimetic enzyme for the construction of an electrochemical biosensor to highly sensitively and simultaneously detect DA and UA. The biosensor modified with the Ru-Ala-C_3N_4 biomimetic enzyme demonstrates excellent electrocatalytic performance, effective electron transfer capability, and high sensitivity compared with previously reported materials in the sensing of DA and UA. The perfect biomimetic enzyme activity of the Ru-Ala-C_3N_4 achieves the simultaneous electrochemical determination of DA and UA with a wide linear concentration range (0.06−490 and 0.5−2135 μM, respectively) and relatively better detection limits (20 and 170 nM, respectively). Besides, the prepared biosensor behaves with good sensitivity, selectivity, and precision and can effectively detect DA and UA in real biological serum samples. It is expected that the single-atom catalysts could be extended to explore physiological processes in complex biological systems as well as disease diagnosis and drug discovery.

ASSOCIATED CONTENT

Supporting Information

The Supporting Information is available free of charge at https://pubs.acs.org/doi/10.1021/acs.analchem.0c05191.

XPS wide scan survey of Ru-Ala-C_3N_4; XRD pattens of samples and BET of Ru-Ala-C_3N_4 and Ru-C_3N_4; cyclic voltammetry curves of Ru-Ala-C_3N_4, Ru-C_3N_4, Ala-C_3N_4, and C_3N_4 with 100 μM DA and 200 μM UA; current response of Ru-Ala-C_3N_4 toward 100 μM DA and 200 μM UA in 0.1 M PBS with different pH values from 6.5 to 9.0; amperometric response of Ru-Ala-C_3N_4 for sample detection (PDF)

AUTHOR INFORMATION

Corresponding Authors

Qunfang Li − *School of Chemical and Environmental Engineering, Hubei Minzu University, Enshi 445000, P.R. China*; Email: slindar809@126.com

Hong Bin Yang − *Institute of Materials Science & Devices, Suzhou University of Science and Technology, Suzhou 215009, P.R. China*; Email: yanghb@usts.edu.cn

Fang Xin Hu − *Institute of Materials Science & Devices, Suzhou University of Science and Technology, Suzhou 215009, P.R. China*; orcid.org/0000-0002-5512-5076; Email: hufx278@usts.edu.cn

Authors

Xiaoli Xie − *School of Chemical and Environmental Engineering, Hubei Minzu University, Enshi 445000, P.R. China; Institute of Materials Science & Devices, Suzhou University of Science and Technology, Suzhou 215009, P.R. China*

https://dx.doi.org/10.1021/acs.analchem.0c05191
Anal. Chem. 2021, 93, 4916−4923

Dong Ping Wang − *Suzhou Institute of Biomedical Engineering and Technology, Chinese Academy of Sciences, Suzhou 215163, P.R. China*
Chunxian Guo − *Institute of Materials Science & Devices, Suzhou University of Science and Technology, Suzhou 215009, P.R. China;* orcid.org/0000-0002-2603-7181
Yuhang Liu − *Institute of Materials Science & Devices, Suzhou University of Science and Technology, Suzhou 215009, P.R. China*
Qianghai Rao − *Institute of Materials Science & Devices, Suzhou University of Science and Technology, Suzhou 215009, P.R. China*
Fangming Lou − *School of Chemical and Environmental Engineering, Hubei Minzu University, Enshi 445000, P.R. China*
Qiannan Li − *School of Chemical and Environmental Engineering, Hubei Minzu University, Enshi 445000, P.R. China*
Yongqiang Dong − *MOE Key Laboratory for Analytical Science of Food Safety and Biology, Fujian Provincial Key Laboratory of Analysis and Detection Technology for Food Safety, College of Chemistry, Fuzhou University, Fuzhou 350000, P.R. China*

Complete contact information is available at: https://pubs.acs.org/10.1021/acs.analchem.0c05191

Author Contributions

F.X.H., H.B.Y., and Q.L. conceived the research and designed the experiments. X.X. performed the experiments and collected the data, partly assisted by D.P.W., C.G., Y.L., Q.R., F.L., Q.L., and Y.D. All of the authors participated in the research. X.X., F.X.H., H.B.Y., and Q.L. discussed the results and wrote the manuscript.

Notes

The authors declare no competing financial interest.

■ ACKNOWLEDGMENTS

We greatly thank the National Natural Science Foundation of China (NO. 21705115, 21665009, 22075195, 21972102), the Natural Science Foundation of Jiangsu Province of China (BK20170378), the Natural Science Research Foundation of Jiangsu Higher Education Institutions (17KJB150036), the Jiangsu Specially-Appointed Professor program for H.B.Y., and the Jiangsu Laboratory for Biochemical Sensing and Biochip for financial support.

■ REFERENCES

(1) Yang, J.; Hu, Y.; Li, Y. C. *Biosens. Bioelectron.* **2019**, *135*, 224−230.
(2) Wang, C.; Yuan, R.; Chai, Y. Q.; Chen, S. H.; Zhang, Y.; Hu, F. X.; Zhang, M. H. *Electrochim. Acta* **2012**, *62*, 109−115.
(3) Argüello, J.; Leidens, V. L.; Magosso, H. A.; Ramos, R. R.; Gushikem, Y. *Electrochim. Acta* **2008**, *54*, 560−565.
(4) Feng, J.; Li, Q.; Cai, J. H.; Yang, T.; Chen, J. H.; Hou, X. M. *Sens. Actuators, B* **2019**, *298*, 126872.
(5) Bhakta, A.; Mascarenhas, R.; D'Souza, O.; Satpati, A.; detriche, S.; Mekhalif, Z.; Dalhalle, J. *Mater. Sci. Eng., C* **2015**, *57*, 328−37.
(6) Li, Q. Z.; Qiu, Y. L.; Han, W. N.; Zheng, Y. Q.; Wang, X. Y.; Xiao, D. D.; Mao, M.; Li, Q. *RSC Adv.* **2018**, *8*, 25808−25814.
(7) Kwon, W.; Kim, J. Y.; Suh, S.; In, M. K. *Forensic Sci. Int.* **2012**, *221*, 57−64.
(8) Alizadeh, N.; Salimi, A. *Anal. Chim. Acta* **2019**, *1091*, 40−49.
(9) Zhuo, S. J.; Fang, J.; Wang, J.; Zhu, C. Q. *Methods Appl. Fluoresc.* **2020**, *8*, 015005.
(10) Rashid, N. C. A.; Ngajikin, N. H.; Azmi, A. I.; Arsat, R.; Isaak, S.; Cholan, N. A.; Azmi, N. E. *Chin. Opt. Lett.* **2019**, *17*, 70−74.
(11) Lou, F. M.; Li, Q. F.; Tang, D. P. *Chem. Lett.* **2015**, *44*, 539−541.
(12) Li, Q.; Tang, D.; Lou, F.; Yang, X.; Chen, G. *ChemElectroChem* **2014**, *1*, 441.
(13) Hu, F. X.; Hu, T.; Chen, S.; Wang, D.; Rao, Q.; Liu, Y.; Dai, F.; Guo, C.; Yang, H. B.; Li, C. M. *Nano-Micro Lett.* **2021**, *13*, 7.
(14) Zhao, S. F.; Hu, F. X.; Shi, Z. Z.; Fu, J. J.; Chen, Y.; Dai, F. Y.; Guo, C. X.; Li, C. M. *Nano Res.* **2021**, *14*, 879−886.
(15) Gan, L.; Tao, H. S.; Kan, X. W.; Chen, Q.; Sheng, K.; Wu, J. J. *J. Anal. Chem.* **2018**, *73*, 978−985.
(16) Matsoso, B. J.; Lerotholi, T.; Coville, N. J.; Jones, G. *Johnson Matthey Technol. Rev.* **2019**, *63*, 76−88.
(17) Savk, A.; Ozdil, B.; Demirkan, B.; Nas, M. S.; Calimli, M. H.; Alma, M. H.ı; Inamuddin; Asiri, A. M.; Sen, F. *Mater. Sci. Eng., C* **2019**, *99*, 248−254.
(18) Sheng, Z. H.; Zheng, X. Q.; Xu, J. Y.; Bao, W. J.; Wang, F. B.; Xia, X. H. *Biosens. Bioelectron.* **2012**, *34*, 125−131.
(19) Wang, Z. H.; Guo, H. J.; Gui, R. J.; Jin, H.; Xia, J. F.; Zhang, F. F. *Sens. Actuators, B* **2018**, *255*, 2069−2077.
(20) Ulubay, Ş.; Dursun, Z. *Talanta* **2010**, *80*, 1461−1466.
(21) He, W. Y.; Ding, Y.; Zhang, W. Q.; Ji, L. F.; Zhang, X.; Yang, F. C. J. *Electroanal. Chem.* **2016**, *775*, 205−211.
(22) Ouyang, X. Q.; Luo, L. Q.; Ding, Y. P.; Liu, B. D.; Xu, D.; Huang, A. Q. J. *Electroanal. Chem.* **2015**, *748*, 1−7.
(23) Zhang, L.; Yang, D. *Electrochim. Acta* **2014**, *119*, 106−113.
(24) Selvaraju, T.; Ramaraj, R. J. *J. Appl. Electrochem.* **2003**, *33*, 759−762.
(25) Liu, C.; Yang, L. Z.; Song, F.; Jiang, L. Y.; Lu, G. H. *Chin. Chem. Lett.* **2005**, *16*, 237−240.
(26) Safavi, A.; Maleki, N.; Moradlou, O.; Tajabadi, F. *Anal. Biochem.* **2006**, *359*, 224−229.
(27) Serra-Pérez, E.; Ferronato, C.; Giroir-Fendler, A.; Álvarez-Torrellas, S.; Ovejero, G.; García, J. *Ind. Eng. Chem. Res.* **2020**, *59*, 15515−15530.
(28) Wang, X. Y.; Li, L. L.; Fang, Z. P.; Zhang, Y. F.; Ni, J.; Lin, B. Y.; Zheng, L. R.; Au, C.-T.; Jiang, L. L. *ACS Catal.* **2020**, *10*, 9504−9514.
(29) Wang, H.; Xu, D. Y.; Guan, E. J.; Wang, L.; Zhang, J.; Wang, C. T.; Wang, S.; Xu, H.; Meng, X. J.; Yang, B.; Gates, B. C.; Xiao, F.-S. *ACS Catal.* **2020**, *10*, 6299−6308.
(30) Mori, K.; Taga, T.; Yamashita, H. *ACS Catal.* **2017**, *7*, 3147−3151.
(31) Li, P.; Wang, M.; Duan, X.; Zheng, L.; Cheng, X.; Zhang, Y.; Kuang, Y.; Li, Y.; Ma, Q.; Feng, Z.; Liu, W.; Sun, X. *Nat. Commun.* **2019**, *10*, 1711.
(32) Cao, L. L.; Luo, Q. Q.; Chen, J. J.; Wang, L.; Lin, Y.; Wang, H. J.; Liu, X. K.; Shen, X. Y.; Zhang, W.; Liu, W.; Qi, Z. M.; Jiang, Z.; Yang, J. L.; Yao, T. *Nat. Commun.* **2019**, *10*, 4849.
(33) Zhao, Z. L.; Wang, Q.; Huang, X.; Feng, Q.; Gu, S.; Zhang, Z.; Xu, H.; Zeng, L.; Gu, M.; Li, H. *Energy Environ. Sci.* **2020**, *13*, 5143−5151.
(34) Lu, B. Z.; Guo, L.; Wu, F.; Peng, Y.; Lu, J. E.; Smart, T. J.; Wang, N.; Finfrock, Y. Z.; Morris, D.; Zhang, P.; Li, N.; Gao, P.; Ping, Y.; Chen, S. W. *Nat. Commun.* **2019**, *10*, 631.
(35) Qin, J. N.; Barrio, J.; Peng, G.; Tzadikov, J.; Abisdris, L.; Volokh, M.; Shalom, M. *Nat. Commun.* **2020**, *11*, 4701.
(36) Gao, J. J.; Yang, H. B.; Huang, X.; Hung, S.-F.; Cai, W. Z.; Jia, C. M.; Miao, S.; Chen, H. M.; Yang, X. F.; Huang, Y. Q.; Zhang, T.; Liu, B. *Chem.* **2020**, *6*, 658−674.
(37) Yang, H. B.; Huang, S.-F.; Liu, S.; Yuan, K. D.; Miao, S.; Zhang, L. P.; Huang, X.; Wang, H.-Y.; Cai, W. Z.; Huang, Y. Q.; Zhang, T.; Liu, B.; et al. *Nat. Energy* **2018**, *3*, 140−147.
(38) Li, B. B.; Zhou, Y. S.; Wu, W.; Liu, M.; Mei, S. R.; Zhou, Y. K.; Jing, T. *Biosens. Bioelectron.* **2015**, *67*, 121−128.
(39) Lei, Y.; Butler, D.; Lucking, M. C.; Zhang, F.; Xia, T. N.; et al. *Sci. Adv.* **2020**, *6*, No. eabc4250.

(40) Wang, C.; Yuan, R.; Chai, Y. Q.; Zhang, Y.; Hu, F. X.; Zhang, M. H. *Biosens. Bioelectron.* **2011**, *30*, 315−319.
(41) Zhang, X.; Zhang, Y. C.; Ma, L. X. *Sens. Actuators, B* **2016**, *227*, 488−496.
(42) Demirkan, B.; Bozkurt, S.; Şavk, A.; Cellat, K.; Gülbağca, F.; Nas, M. S.; Alma, M. H.; Sen, F. *Sci. Rep.* **2019**, *9*, 12258.
(43) Demirkan, B.; Bozkurt, S.; Cellat, K.; Arkan, K.; Ylmaz, M.; Avk, A.; Alml, M. H.; Nas, M. S.; Atalar, M. N.; Alma, M. H.; et al. *Sci. Rep.* **2020**, *10*, 2946.
(44) Ma, L.; Zhang, Q. R.; Wu, C.; Zhang, Y.; Zeng, L. T. *Anal. Chim. Acta* **2019**, *1055*, 17−25.
(45) Guo, Z.; Luo, X. K.; Li, Y. H.; Li, D. D.; Zhao, Q. N.; Li, M. M.; Ma, C.; Zhao, Y. T. *Chem. Res. Chin. Univ.* **2017**, *33*, 507−512.
(46) Wang, M. L.; Cui, M. Z.; Liu, W. F.; Liu, X. G. J. *Electroanal. Chem.* **2019**, *832*, 174−181.
(47) Jafari, H.; Ganjali, M. R.; Dezfuli, A. S.; Faridbod, F. *Appl. Surf. Sci.* **2018**, *427*, 496−506.
(48) Zhao, D. Y.; Yu, G. L.; Tian, K. L.; Xu, C. X. *Biosens. Bioelectron.* **2016**, *82*, 119−126.
(49) Wang, C. Q.; Du, J.; Wang, H. W.; Zou, C. E.; Jiang, F. X.; Yang, P.; Du, Y. X. *Sens. Actuators, B* **2014**, *204*, 302−309.

https://dx.doi.org/10.1021/acs.analchem.0c05191
Anal. Chem. 2021, 93, 4916−4923